

UC Davis

UC Davis Previously Published Works

Title

Reduced brain oxygen metabolism in patients with multiple sclerosis: Evidence from dual-calibrated functional MRI.

Permalink

<https://escholarship.org/uc/item/7gb1q7zd>

Journal

Cerebrovascular and brain metabolism reviews, 43(1)

Authors

Chandler, Hannah

Stickland, Rachael

Patitucci, Eleonora

et al.

Publication Date

2023

DOI

10.1177/0271678X221121849

Copyright Information

This work is made available under the terms of a Creative Commons Attribution License, available at <https://creativecommons.org/licenses/by/4.0/>

Peer reviewed

Reduced brain oxygen metabolism in patients with multiple sclerosis: Evidence from dual-calibrated functional MRI

Journal of Cerebral Blood Flow & Metabolism
2023, Vol. 43(1) 115–128
© The Author(s) 2022
Article reuse guidelines:
sagepub.com/journals-permissions
DOI: 10.1177/0271678X221121849
journals.sagepub.com/home/jcbfm



Hannah L Chandler^{1,†}, Rachael C Stickland^{1,2,†} ,
Eleonora Patitucci^{1,†}, Michael Germuska¹ ,
Antonio M Chiarelli^{3,4} , Catherine Foster^{1,5},
Shona Bhome-Dhaliwal⁶, Thomas M Lancaster^{1,7},
Neeraj Saxena^{1,8}, Sharmila Khot^{1,6},
Valentina Tomassini^{1,3,4,9,10,11,*} and Richard G Wise^{1,3,4,*}

Abstract

Cerebral energy deficiency is increasingly recognised as an important feature of multiple sclerosis (MS). Until now, we have lacked non-invasive imaging methods to quantify energy utilisation and mitochondrial function in the human brain. Here, we used novel dual-calibrated functional magnetic resonance imaging (dc-fMRI) to map grey-matter (GM) deoxy-haemoglobin sensitive cerebral blood volume (CBV_{dHb}), cerebral blood flow (CBF), oxygen extraction fraction (OEF), and cerebral metabolic rate of oxygen consumption (CMRO₂) in patients with MS (PwMS) and age/sex matched controls. By integrating a flow-diffusion model of oxygen transport, we evaluated the effective oxygen diffusivity of the capillary network (D_C) and the partial pressure of oxygen at the mitochondria (PmO₂). Significant between-group differences were observed as decreased CBF ($p = 0.010$), CMRO₂ ($p < 0.001$) and D_C ($p = 0.002$), and increased PmO₂ ($p = 0.043$) in patients compared to controls. No significant differences were observed for CBV_{dHb} ($p = 0.389$), OEF ($p = 0.358$), or GM volume ($p = 0.302$). Regional analysis showed widespread reductions in CMRO₂ and D_C for PwMS. Our findings may be indicative of reduced oxygen demand or utilisation in the MS brain and mitochondrial dysfunction. Our results suggest changes in brain physiology may precede MRI-detectable GM loss and may contribute to disease progression and neurodegeneration.

Keywords

Multiple sclerosis, neurodegeneration, disability, cerebral blood flow, cerebral oxygen consumption

Received 20 January 2022; Revised 1 June 2022; Accepted 21 July 2022

¹CUBRIC, School of Psychology, Cardiff University, Cardiff, UK

²Department of Physical Therapy and Human Movement Sciences, Northwestern University, Chicago, IL, USA

³Institute for Advanced Biomedical Technologies, University “G. d’Annunzio” of Chieti-Pescara, Chieti, Italy

⁴Department of Neurosciences, Imaging and Clinical Sciences, University “G. d’Annunzio” of Chieti-Pescara, Chieti, Italy

⁵Wales Institute of Social and Economic Research and Data, Cardiff University, Cardiff, UK

⁶Cardiff University School of Medicine, Cardiff, UK

⁷Department of Psychology, University of Bath, Bath, UK

⁸Department of Anaesthetics, Intensive Care and Pain Medicine, Cwm Taf Morgannwg University Health Board, Abercynon, UK

⁹MS Centre, Neurology Unit, “SS. Annunziata” University Hospital, Chieti, Italy

¹⁰Division of Psychological Medicine and Clinical Neurosciences, School of Medicine, Cardiff University, Cardiff, UK

¹¹Helen Durham Centre for Neuroinflammation, University Hospital of Wales, Cardiff, UK

[†]Equal contribution (first author), ^{*}Equal contribution (senior author).

Corresponding author:

Richard G Wise, Institute for Advanced Biomedical Technologies (ITAB), Department of Neurosciences, Imaging and Clinical Sciences, University “G. D’Annunzio” of Chieti-Pescara, Chieti, Italy.
Email: richard.wise@unich.it

Introduction

Altered blood supply and energy metabolism are pervasive features of multiple sclerosis (MS).^{1,2} A reduction in cerebral blood flow (CBF) is thought to precede lesion formation,³ and can occur in the absence of significant tissue volume loss.⁴ Changes in cerebrovascular reactivity (CVR) occur in MS, correlating with the degree of tissue damage.^{5–7} In parallel with changes in brain energy supply, indexed by CBF, reductions in brain energy consumption have been detected using 2-[¹⁸F]FDG and ¹⁵O-PET^{8–11} and related to cognitive dysfunction in MS.¹² This evidence suggests a malfunction of the neurovascular unit that reflects an altered capacity for energy utilisation in the MS brain, in addition to a hypoxic-like tissue state, that may be linked to inflammation and chronically may lead to further tissue damage^{13–17} and disability.^{2,18} The relationship between altered brain blood flow and oxygen consumption in MS, however, remains to be elucidated. Additional information is required to identify whether reduced vascular function may be limiting energy consumption or if reduced vascular performance is secondary to reduced energy demand or the ability of the tissue to access and use metabolic substrates.

Studies mapping the effects of MS inflammation on brain energy consumption in humans have so far been limited to PET. However, the development of novel multi-parametric MRI methods that map relevant physiological parameters across the cortex can provide insight into the disease processes that contribute to tissue damage and disability. Dual-calibrated fMRI (dc-fMRI) methods^{19–22} have demonstrated their ability to quantitatively map grey matter (GM) deoxyhemoglobin sensitive cerebral blood volume (CBV_{dHb}), cerebral blood flow (CBF), oxygen extraction fraction (OEF) and cerebral metabolic rate of oxygen consumption (CMRO₂)^{23–26} in both healthy and clinical cohorts²⁷ and with pharmacological intervention.²⁸

In this study, using dc-fMRI, we quantify and map cerebral grey matter (GM) vascular and O₂ metabolic function in patients with relapsing-remitting MS (PwMS) and in healthy controls, under the hypothesis of a generalised dysregulation in GM physiology in the patients. We also investigate the relationship between measures of oxygen metabolic function and metrics of damage and disability, expecting a relationship between brain physiology and structural and clinical measures. Furthermore, by integrating a flow-diffusion model of oxygen transport, we evaluate the effective oxygen diffusivity of the capillary network (D_C) and the partial pressure of oxygen at the mitochondria (PmO₂). This could provide a critical advance in our understanding of the contribution of hypoxia in MS pathophysiology and its association with altered

energy utilisation and mitochondrial dysfunction. This non-invasive MRI study aims to improve our understanding of the pathophysiological mechanisms of tissue dysfunction and damage in relapsing-remitting multiple sclerosis.

Materials and methods

Participants

We recruited PwMS (n = 22) and age and sex matched healthy controls (n = 20) of mixed handedness. All patients (age range: 27–45 years) were recruited at the University Hospital of Wales in Cardiff, UK. All PwMS had a diagnosis of MS²⁹ with a relapsing-remitting course.³⁰ Eligibility criteria for PwMS included no change in medication and no relapse or steroid treatment in the 3 months prior to study entry. Participants had no history (within the preceding 2 years) of, or were being treated for, any significant cardiac or respiratory disease, and were not regular smokers in the preceding 6 months. Data collection was conducted at Cardiff University Brain Research Imaging Centre (CUBRIC, Cardiff University).

Data collection

Clinical data and behavioural assessments. Participants completed a socio-demographic and lifestyle questionnaire. Tests from the MS Functional Composite³¹ were carried out on all participants: 9-Hole Peg Test (9-HPT) for upper limb function, Timed 25-Foot Walk (T25-FW) for leg function/ambulation, the Paced Auditory Serial Addition Test (PASAT) 2 and 3 seconds as a measure of cognitive function. The Symbol Digit Modalities Test (SDMT) was also used to assess cognitive function.³² Visual acuity was assessed, in each eye separately, with a SLOAN letter chart (*Precision Vision*) at 100% contrast and scored in two ways: (1) the smallest letter size (in M-units) at which 3 out of 5 letters were correctly read, and (2) a cumulative score of total letters read, out of 60. Participants were tested with corrected vision. For patients only, disability and disease impact were assessed with the Multiple Sclerosis Impact Scale (MSIS-29)³³ and the Fatigue Scale for Motor and Cognitive Functions (FSMC).³⁴ Clinical records and a short interview on disease history and impact gave information on: disease onset, relapse history, and Expanded Disability Status Scale (EDSS) score.³⁵

MRI acquisitions

All MRI data were acquired on Siemens Prisma 3T MRI scanner (*Siemens Healthineers, Erlangen, Germany*), using a 32-channel receive-only head coil.

Structural scans

A magnetisation-prepared rapid acquisition with gradient echo (MPRAGE) T1-weighted scan was used for registration and brain segmentation purposes (matrix $165 \times 203 \times 197$, 1 mm isotropic resolution, TR/TE = 2100/3.24 ms). A 3D T2-weighted Fluid Attenuated Inversion Recovery (FLAIR) image (1 mm isotropic resolution, 256 slices, TR/TE = 5000/388 ms) and T2/Proton Density dual-echo image (in-plane resolution 0.8×0.8 mm, 41 slices, 3.9 mm thick, TR/TE1/TE2 = 4050/11/90 ms) were acquired for lesion identification and contouring.

Quantitative functional scans

In order to map the O_2 consumption and the cerebrovascular function across the GM with dc-fMRI, CBF and BOLD signals were concurrently acquired using a home-written dual-excitation³⁶ PCASL-based acquisition sequence with background suppression and pre-saturation^{19,37} that acquires CBF and BOLD signals together to map changes in O_2 consumption and cerebrovascular function across the GM. Scan parameters were: TE1 = 10 ms, TE2 = 30 ms, TR = 4400 ms, in-plane resolution 3.4×3.4 mm, 16 slices with 7 mm thickness and 20% slice gap, GRAPPA acceleration factor 3 (Figure 1). The acquisition time for the PCASL sequence was 18 minutes, during which interleaved periods of hypercapnic and hyperoxic gas mixtures were delivered to participants using a facemask.^{19,26} Hypercapnic periods involved delivering 5% carbon dioxide (CO_2), whereas, for hyperoxia, 50% O_2 was delivered, with short periods of 100% O_2 at the start and 10% O_2 at the end in order to accelerate the transitions to the hyperoxic state and back to normoxia. Physiological monitoring was conducted through measurement of the heart rate (HR) and peripheral O_2 (%) saturation (Medrad, Pittsburgh, PA). Partial pressures of end-tidal O_2 ($P_{ET}O_2$) and CO_2 ($P_{ET}CO_2$) were measured from expired gases sampled from the participant's facemask using an AD Instruments gas analyser and data

sampling system (PowerLab®, ADInstruments, Sydney, Australia). A blood sample was drawn within the hour before the start of the MRI scan via a finger prick with a 1.8 mm lancet and analysed with the HemoCue® Hb 301 + system in accordance with the manufacturer's guidelines (Hemo Ängelholm, Sweden). This gave a reading of blood haemoglobin concentration ([Hb]) in grams per litre (g/L) for use in the calculation of OEF.

Data analysis

We performed lesion filling in PwMS to permit accurate GM identification through tissue segmentation and thus extract cerebral physiological parameters representative of the GM. We restricted our analysis of functional data to voxels containing mainly GM in order to limit the effect of any potential GM loss in the PwMS. A biophysical model was applied to the BOLD-ASL signals to estimate voxel-wise physiological parameters in the GM. We conducted a region-wise analysis of physiological parameters to further reduce sensitivity to GM partial volume errors associated with tissue loss and to enhance sensitivity through regional averaging. All MRI data were pre-processed and analysed using an in-house written MATLAB (R2015a) pipeline and FSL.³⁸ Segmentation of GM and WM was performed with a combination of FSL-FAST³⁹ and FSL-FIRST⁴⁰ for subcortical structures (see below). Registrations were carried out with FSL-FLIRT⁴¹ and non-brain removal with BET.⁴²

Lesion filling

T2, PD and FLAIR images were brain extracted. The T2-FLAIR image was transformed to the same space as T2-PD image. All three image contrasts were used to locate the lesions. Using JIM (Version 6.0), lesions were defined manually on the T2-PD images using the contour ROI tool, without 3D propagation. This lesion map was exported as a NIFTI file, with a pixel area threshold of 50% and a total lesion volume was calculated for each PwMS. For the lesion filling of the

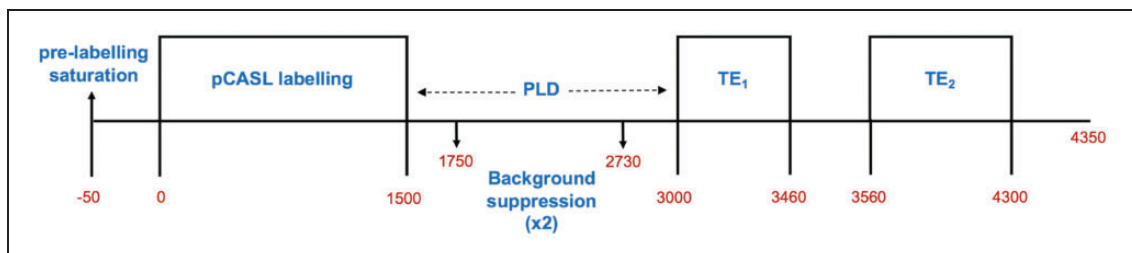


Figure 1. Graphical representation of the sequence parameters and timings (ms) for dc-fMRI dual-excitation sequence. TE₁ represents the block of slices acquired for ASL weighted signal, whereas TE₂ represents the block of slices acquired for BOLD weighted signal. TE: Echo time; PLD: post label delay; pCASL: pseudo continuous arterial spin labelling.

T1 weighted image, the PD image was registered to the T1 image, and the lesion map was binarised and transformed to T1-space. The lesion map was thresholded at 0.4 to approximately preserve the size of the original lesion map after transformation and to allow a small amount of inflation, in case of registration errors. This map was then binarised. The function *lesion_filling*⁴³ was used: this fills the lesion area with intensities similar to those of the non-lesion neighbourhood.⁴⁴

GM and WM volumes

Using the lesion-filled T1 image, FSL-FAST was run. Segmentation was used to investigate differences in GM and WM volume between groups. GM, WM and CSF partial volume estimates (PVE) were created through FAST (FSL tool) segmentation of the T1-weighted image. A probability threshold of 0.5 was used to identify GM and WM voxels for each participant. To account for different head sizes when calculating differences in GM and WM volume, we normalised these measures to intracranial volume (ICV). ICV was calculated with the use of FSL (<http://fsl.fmrib.ox.ac.uk>) following the ENIGMA protocol (<https://enigma.ini.usc.edu/protocols/imaging-protocols/protocol-for-brain-and-intracranial-volumes/>).⁴⁵ ENIGMA is an atlas-based estimation procedure where: i) the subject structural image is linearly aligned to MNI152 standard space; ii) ICV is calculated by multiplying the inverse of the determinant of the affine matrix by the size of the template (MNI152) brain. Overall, this analysis allowed us to assess whether possible GM volume differences are associated with differences in vascular and metabolic function in the PwMS compared to the controls.

dc-fMRI modelling

Analysis of the dc-fMRI data was conducted using a Frequency-domain Machine Learning (FML) method.²⁴ The method takes advantage of the speed and noise resilience of artificial neural networks to make rapid and robust parameter estimates without the need to apply spatial smoothing. Once the FML pipeline had been run for each participant, the output maps (CBV_{dHB} ml/100 g, CBF ml/100 g/min, OEF, $CMRO_2$ μ mol/100 g/min) were analysed in each subject's dc-fMRI space. Functional data (TE1, first echo) was registered to the structural T1-weighted image using FSL's *epi-reg* tool. Using the inverse of this matrix, the T1-image and the GM-PVE image were transformed to functional space. The GM-PVE image (thresholded at 0.5) was binarised and used as a GM mask for calculating whole-GM and

regional-GM parameter estimates from the FML output maps (median values). To reduce the effect of GM loss that may bias the cerebral physiological parameters, we performed the analysis restricting our estimate of physiological parameters to voxels which contain a majority of GM. We applied two different pipelines to achieve good segmentation of cortical and subcortical structures. We used FAST to define cortical GM ($PVE > 0.5$) and intersected it with the automated anatomical labelling (AAL) atlas to identify cortical regions. For subcortical regions we instead used FIRST⁴⁰ to provide accurate segmentation of those structures ($PVE > 0.5$). From here, statistical analysis was run to identify group differences in CBF, OEF and $CMRO_2$. D_C (μ mol/100g/mmHg/min) was calculated using GM median values of OEF and $CMRO_2$, using a flow-diffusion model of oxygen transport with the procedure presented in Germuska (2019).²⁵ PmO_2 (mmHg) was obtained by further expanding the diffusion modelling and assuming an effective tissue permeability to oxygen of $k = 3 \mu$ mol/mmHg/ml/min and the ratio of CBV_{dHB} and capillary blood volume of $\rho = 2$.⁴⁶ PmO_2 was estimated implementing a grid search approach with a large search range (-200 – 200 mmHg, negative values were allowed to avoid bias).

Regional analysis

In addition to the global GM analysis we also applied the two different cortical and subcortical segmentation pipelines to the regional analysis (see above for further details). Registration matrices were defined between dc-fMRI space and MNI space, using FSL's FLIRT (linear) function. Registration between native and standard space involved registering the T1 structural image to MNI space using a standard template. The inverse of this matrix for each participant was used to transform the AAL atlas to native dc-fMRI space,⁴⁷ where vascular/metabolic parameters were extracted for each cortical region. Due to the limited number of slices in our dc-fMRI acquisition, it was not possible to include the cerebellum in the analysis. We also excluded Heschl's gyrus (L & R), and the superior temporal (L & R) regions, due to low BOLD signal in the raw data around the sinuses. This left 74 cortical regions of interest. Subcortical regions segmented included bilateral Thalamus, Caudate, Putamen, Pallidum, Hippocampus, Amygdala, Accumbens and brain stem. Median values for each parameter (CBV_{dHB} , CBF, OEF, and $CMRO_2$) were extracted from each region. Regional D_C values were calculated using the median values for regional OEF and $CMRO_2$.²⁵ Due to the high level of noise in the PmO_2 measurement,

regional analysis was not possible, and instead we report this measurement as a global GM marker.

Partial volume estimate analysis

To assess whether differences in the physiological parameters vary with the proportion of GM present in the voxels, we ran a partial volume estimate (PVE) analysis. Binarised masks were created from the GM PVE in individual subject functional space for different GM PVE ranges (7 bins of equal width from 0.1–0.8). Within each mask for each parameter (CBF, OEF and CMRO₂), median values were calculated. D_C was calculated using median values of OEF and CMRO₂ in each GM PVE range.

Statistical analysis

Demographic and clinical data: Independent sample *t*-tests were run between groups for each of the demographic, cognitive and behavioural measures. For demographics including sex, a chi squared (X²) test was run. *Grey matter/White matter volumes:* between-group differences in global normalised WM and GM volumes were investigated using independent samples *t*-tests. *Grey matter dc-fMRI analysis:* From here, independent samples *t*-tests were used to test for differences between patients and controls in CBV_{dHb}, CBF, OEF, CMRO₂, D_C and PmO₂, for both cortical and subcortical GM. We included CSF volume estimates as a covariate. *Regional analysis:* statistical analysis involved running *t*-tests between patients and controls for each region (FDR corrected) using custom R and Python scripts. *Partial volume estimate analysis:* a mixed ANOVA was run to look at main effects (GM PVE bin; Group) and interaction effects (GM PVE bin*Group). *Grey and white matter volumes:* *t*-tests were carried out to investigate between-group differences in global WM and GM volumes. We used correlation analysis to test the relationship between brain physiological parameters and levels of disability. Shapiro-Wilks test was used to assess normality of the data. All *p*-values reported are 2-tailed. R version 3.6.1. was used for all statistical analyses (<http://www.rstudio.com/>).

Standard protocol approvals, registrations, and patient consents

Written informed consent was obtained from all PwMS and healthy volunteers. The study was approved by the NHS Research Ethics Committee, Wales, UK and Cardiff University's Ethics Committee, School of

Psychology, Cardiff, UK, in accordance with the Declaration of Helsinki.

Results

Clinical, demographic and tissue volume characteristics

Demographic and clinical characteristics of the two cohorts are shown in Table 1. Significant between-group differences were seen only for the T25-FW ($p=0.006$). There was no significant difference in GM normalised volume ($t(40)=0.76$; $p=0.454$), but patients showed a significantly lower WM normalised volume compared to controls ($t(40)=3.56$; $p<0.001$) (Table 1). There was no significant difference in blood haemoglobin content (g/L) between patients (135.7 ± 3.29 g/L) and controls (136.5 ± 2.83 g/L) [$t(40)=0.19$, $p=0.849$].

Between group differences in GM physiology

Patients had significantly lower global cortical GM CBF [PwMS vs. controls: 43.9 ± 6.1 vs. 48.9 ± 5.9 ml/100 g/min, $t(40)=2.70$, $p=0.010$] and global cortical GM CMRO₂ [PwMS vs. controls: 117.7 ± 17.3 vs. 136.5 ± 14.5 μ mol/100 g/min, $t(40)=3.80$, $p<0.001$] compared to controls (Figure 2). There was no significant group difference in global cortical GM CBV_{dHb} [PwMS vs. controls: 4.20 ± 1.29 ml/100g vs. 4.391 ± 1.99 ml/100g, $t(40)=0.35$, $p=0.389$] and global cortical GM OEF [PwMS vs. controls: 0.38 ± 0.09 vs. 0.39 ± 0.02 , $t(40)=0.93$, $p=0.358$] (Figure 2). When integrating the results with the model of oxygen transport, patients had significantly lower global cortical GM D_C [PwMS vs. controls: 2.70 ± 0.51 vs. 3.18 ± 0.41 μ mol/100 g/mmHg/min, $t(40)=3.32$, $p=0.002$] and higher global cortical PmO₂ [PwMS vs. controls: 9.31 ± 14.2 mmHg vs. 1.03 ± 11.24 mmHg, $t(40)=2.01$, $p=0.043$] compared to controls (Figure 2). We ran a global subcortical GM analysis to investigate between-groups metabolic differences in these structures and did not observe between-groups differences in subcortical GM for any of our metabolic parameters (CBF: $t(40)=1.52$, $p=0.137$; CMRO₂: $t(40)=1.42$, $p=0.164$; D_C: $t(40)=1.25$, $p=0.219$; OEF: $t(40)=1.34$, $p=0.189$, PmO₂: $t(40)=-1.45$, $p=.156$). Due to possible differences in brain volume between groups and consequent differences in the CSF content of voxels, we included the CSF PVE, measured within the voxels classified as GM, as a regressor in our global GM analysis. Our results remained consistent, showing

Table 1. Demographic and clinical characteristics. Values are mean \pm SD, unless stated otherwise. Group differences were tested with t-tests, except for sex, which was tested with chi-squared test.

	Patients	Controls	p
Age	35.55 \pm 7.24	34.15 \pm 5.69	0.489
Sex	5/17 (M/F)	6/14 (M/F)	0.854
Education (years)	17.14 \pm 1.96	18.58 \pm 2.81	0.699
Hemoglobin (g/L)	135.95 \pm 3.15	136.55 \pm 2.83	0.890
Disease duration (years)	8.20 \pm 4.85	—	—
EDSS	2.25 \pm 1.34/range 0–6	—	—
MSIS physical	1.80 \pm 0.80	—	—
MSIS mental	1.88 \pm 0.73	—	—
Number of patients on DMT's	11	—	—
Visual Acuity-L (cumulative)	3.46 \pm 1.17	3.53 \pm 3.06	0.928
Visual Acuity-R (cumulative)	3.25 \pm 1.51	2.88 \pm 1.32	0.402
9HPT-dominant (seconds)	20.98 \pm 4.90	20.18 \pm 2.28	0.235
9HPT-non-dominant (seconds)	22.92 \pm 2.55	21.25 \pm 2.97	0.058
T25-FW (seconds)	5.00 \pm 1.49	3.98 \pm 0.63	0.006
PASAT-3s (correct/60)	44.50 \pm 12.91	48.10 \pm 10.54	0.326
PASAT-2s (correct/60)	34.05 \pm 11.74	35.90 \pm 12.21	0.623
SDMT	59.14 \pm 7.47	62.40 \pm 9.76	0.499
T2 hyperintense lesion volume (mm ³)	101 \pm 9	—	—
White matter volume (ml)	514 \pm 19	537 \pm 23	<.001
Grey matter volume (ml)	536 \pm 26	541 \pm 21	0.454

F: female; M: male; DMTs: disease modifying treatments; EDSS: Expanded Disability Status Scale; MSIS: Multiple Sclerosis Impact Scale; L = left; R: right; 9HPT: 9 Hole Peg Test; T25FW: Timed 25-foot walk; PASAT: Paced Auditory Serial Addition Test; SDMT: Symbol Digit Modality Test.

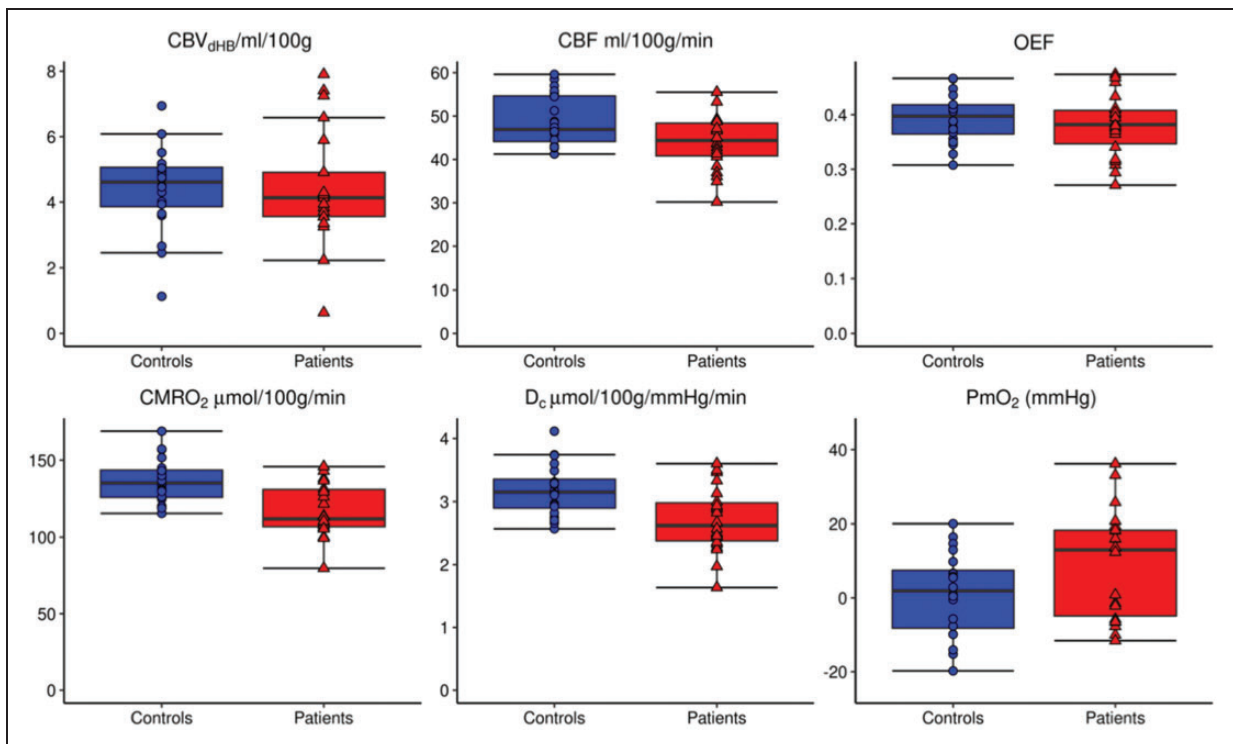


Figure 2. Physiological parameters in PwMS and in controls. CBV_{dHb}, CBF, OEF, CMRO₂, D_c and PmO₂ in patients (red triangles) and in controls (blue circles). Results reflect median values in the GM for each participant (PVE threshold of 0.5). There was a significant difference between groups in CBF, CMRO₂, D_c, and PmO₂, but not in CBV_{dHb} or OEF. GM: grey matter; CBV_{dHb}: grey-matter deoxy-haemoglobin sensitive cerebral blood volume; CBF: cerebral blood flow; OEF: oxygen extraction fraction, CMRO₂: cerebral metabolic rate of oxygen consumption; D_c: capillary oxygen diffusivity; PmO₂: partial pressure of oxygen at the mitochondria.

significant group differences in CBF, CMRO₂ and D_C, but no differences in OEF.

Results of the regional analysis revealed significant widespread reductions in both CMRO₂ and D_C in PwMS compared to controls across cortical GM, but no between-group differences were observed in subcortical structures ($p < 0.05$, FDR corrected) (Figure 3, Table 2). No significant regional group differences were seen for CBV_{dHb}, CBF or OEF ($p > .05$). None of the data violated the assumptions associated with independent samples t-tests.

Relationship between brain physiology and measures of damage and disability

There was a significant negative correlation between white matter T2 hyperintense lesion volume and global cortical GM CBF ($R = -0.52$, $p = 0.014$), as well as between white matter T2 hyperintense lesion volume and global cortical GM CMRO₂ ($R = -0.48$,

$p = 0.023$). There were no significant correlations between T2 lesion volume and global OEF and D_C.

No significant correlations were observed between EDSS scores and global GM CBV_{dHb} ($R = -0.16$, $p = 0.492$), CBF ($R = -0.36$, $p = 0.103$), OEF ($R = -0.12$, $p = 0.606$), CMRO₂ ($R = -0.06$, $p = 0.781$), D_C ($R = 0.16$, $p = 0.492$), or PmO₂ ($R = 0.01$, $p = 0.962$). Similarly, no significant correlations between regional vascular/metabolic parameters and other measures of disability (MSIS, SDMT, PASAT, visual acuity, T25FW) were observed ($p > 0.05$, FDR corrected).

The effect of GM partial volume on physiological parameter estimates

The partial volume analysis of global GM revealed a significant main effect of PVE bin for all parameters CBF, OEF, CMRO₂, and D_C, broadly indicating an increase in the estimate of each parameter with

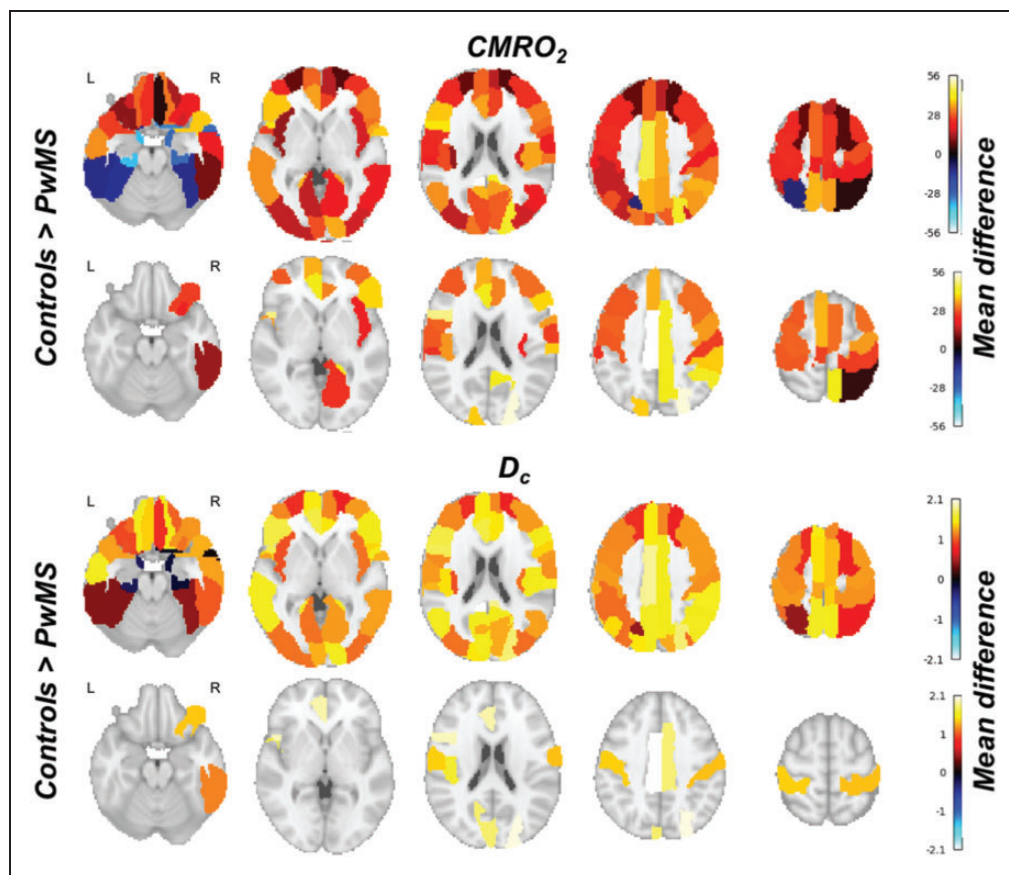


Figure 3. Mean group differences for regional CMRO₂ and D_C. Maps for mean group differences (controls > PwMS) are shown unthresholded (top row) and FDR thresholded ($p < 0.05$) (bottom row) for regional CMRO₂ ($\mu\text{mol}/100\text{g}/\text{min}$) and D_C ($\mu\text{mol}/100\text{g}/\text{mmHg}/\text{min}$). Differences between groups are reported by a colour-coded scale: warm colours indicate regions where controls have greater values than patients; cold colours indicate regions where patients have greater values than controls. Reductions in CMRO₂ and D_C appear to be widespread in patients. PwMS: patients with MS; CMRO₂: cerebral metabolic rate of oxygen consumption; D_C: capillary oxygen diffusivity.

Table 2. Regional analysis. We report the areas in which significant reductions in physiological measures were observed in patients compared to controls. Significant regional differences were found for CMRO₂ and D_C. Results are FDR corrected.

Parameter	Region	t-stat	Cohen's <i>d</i>	CI 2.5%	CI 97.7%	p _{fdr}
CMRO ₂	Cingulum Middle Left	4.06	1.24	0.57	1.92	0.017
CMRO ₂	Inferior Frontal Gyrus, Orbital, Right	3.55	1.08	0.42	1.74	0.024
CMRO ₂	Superior Occipital Gyrus, Right	3.56	1.09	0.43	1.75	0.024
CMRO ₂	Postcentral Gyrus, Right	3.40	1.04	0.38	1.69	0.024
CMRO ₂	Inferior Temporal Gyrus, Right	3.38	1.03	0.37	1.68	0.024
CMRO ₂	Inferior Frontal gyrus, Opercular, Left	3.31	1.01	0.35	1.66	0.024
CMRO ₂	Cingulum Anterior, Left	3.24	0.99	0.34	1.65	0.027
CMRO ₂	Precentral Gyrus, Right	3.17	0.97	0.32	1.62	0.027
CMRO ₂	Rolandic Operculum Left	3.08	0.95	0.30	1.60	0.028
CMRO ₂	Anterior Cingulate, Right	3.04	0.93	0.28	1.57	0.028
CMRO ₂	Postcentral Gyrus, Left	3.08	0.94	0.29	1.59	0.028
CMRO ₂	Precuneus, Right	2.97	0.91	0.26	1.55	0.030
CMRO ₂	SupraMarginal, Right	2.87	0.88	0.23	1.52	0.037
CMRO ₂	Superior Parietal Gyrus, Right	2.82	0.86	0.22	1.51	0.041
CMRO ₂	Supplementary Motor Area, Left	2.74	0.84	0.20	1.48	0.042
CMRO ₂	Superior Occipital Gyrus, Left	2.76	0.85	0.20	1.49	0.042
CMRO ₂	Precentral Gyrus, Left	2.69	0.82	0.18	1.46	0.043
CMRO ₂	Inferior Parietal, Right	2.70	0.83	0.19	1.47	0.043
CMRO ₂	Middle Frontal Gyrus, Left	2.65	0.80	0.16	1.45	0.043
CMRO ₂	Lingual Gyrus, Right	2.65	0.80	0.16	1.44	0.043
CMRO ₂	Middle Frontal Gyrus, Right	2.62	0.80	0.16	1.44	0.043
CMRO ₂	Inferior Frontal Gyrus, Orbital, Right	2.57	0.78	0.14	1.42	0.043
CMRO ₂	Supplementary Motor Area Right	2.52	0.77	0.13	1.41	0.043
CMRO ₂	Superior Frontal Gyrus, Medial, Left	2.53	0.79	0.14	1.45	0.043
CMRO ₂	Insula, Right	2.56	0.79	0.15	1.43	0.043
CMRO ₂	SupraMarginal Left	2.53	0.77	0.13	1.41	0.043
CMRO ₂	Paracentral Lobule, Left	2.57	0.79	0.15	1.43	0.043
CMRO ₂	Middle Cingulum, Right	2.49	0.76	0.13	1.40	0.045
DC	Middle Cingulum, Left	3.83	1.17	0.50	1.84	0.032
DC	Inferior Frontal gyrus, Opercular, Left	3.04	0.93	0.28	1.58	0.040
DC	Inferior Frontal gyrus, Opercular, Right	3.08	0.94	0.29	1.59	0.040
DC	Rolandic Operculum, Left	3.21	0.99	0.34	1.64	0.040
DC	Anterior Cingulum, Left	3.23	0.99	0.34	1.64	0.040
DC	Superior Occipital, Right	3.45	1.06	0.40	1.72	0.040
DC	Postcentral, Right	3.02	0.92	0.27	1.57	0.040
DC	Inferior Temporal Gyrus, Right	3.26	0.99	0.33	1.64	0.040
DC	Middle Cingulum, Right	2.85	0.87	0.23	1.52	0.047
DC	Cuneus, Left	2.87	0.89	0.24	1.55	0.047
DC	Postcentral Gyrus, Left	2.87	0.88	0.23	1.52	0.047

CMRO₂: cerebral metabolic rate of oxygen consumption; D_C: capillary oxygen diffusivity.

increasing proportion of GM (Figure 4 and Table 3). We also observed a significant main effect of Group for CBF, CMRO₂, and D_C, but not for OEF, suggesting consistently lower values of CBF, CMRO₂ and D_C across different GM thresholds in PwMS compared to controls. Finally, there were no significant interactions PVE bin*Group for any of the parameters CBF, OEF, CMRO₂ or D_C (Table 3), indicating that GM thresholds have little influence on detecting physiological differences between PwMS and controls.

To evaluate whether regional GM volume may have contributed to the regional group differences of

physiological parameters, we calculated the number of voxels (PVE threshold >0.5) in each ROI and compared this value between groups. Results showed no significant differences between PwMS and controls in any of the AAL regions ($p > 0.05$, FDR corrected).

Discussion

This study quantifies cerebral blood flow and oxygen consumption in PwMS using a multiparametric MRI method.^{25,26} We observed reductions in global CBF, CMRO₂, and D_C and increases in PmO₂ within the

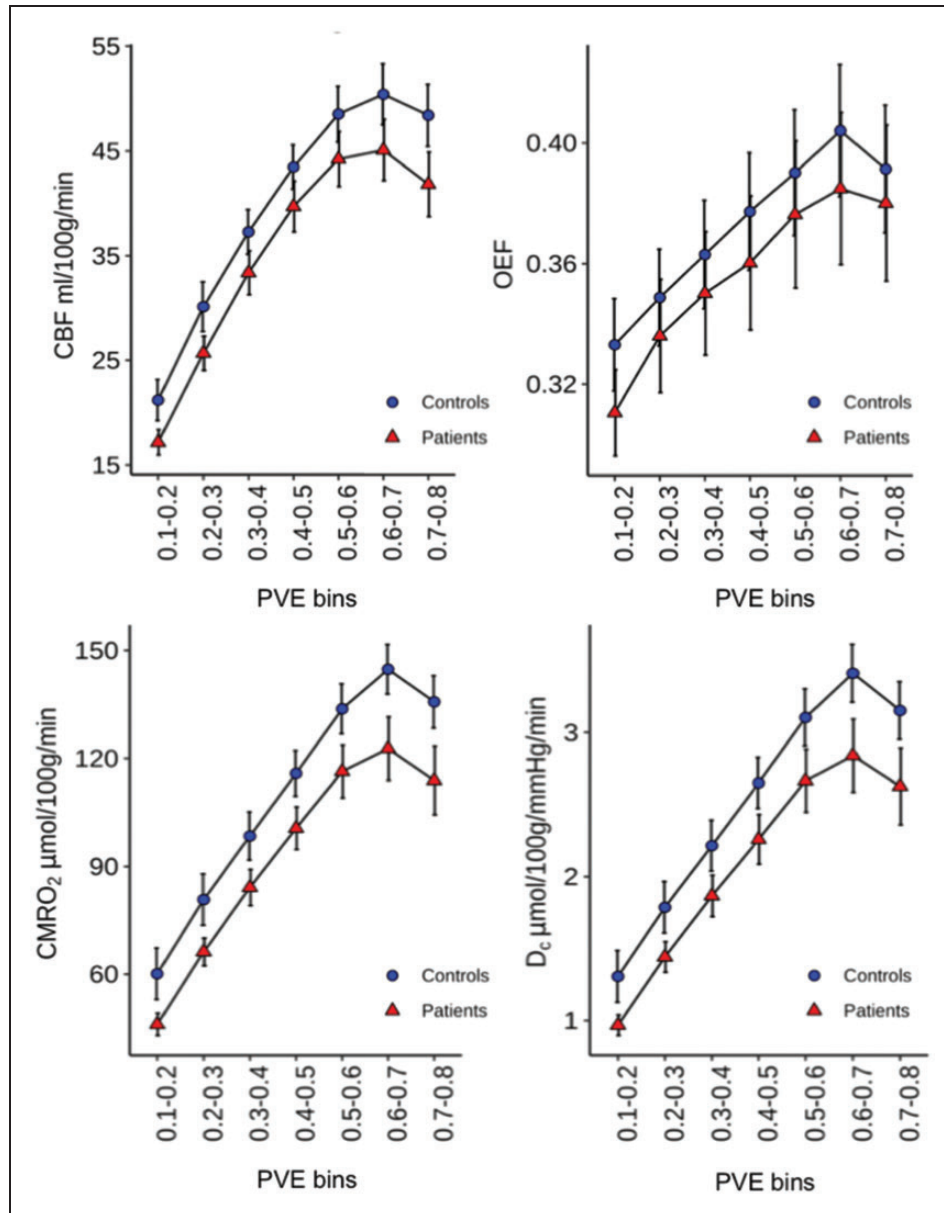


Figure 4. Partial volume analysis for physiological parameters. Mean values of physiological parameters (CBF, OEF, CMRO₂, and D_C) across different PV bins for PwMS (red triangles) and controls (blue circles). Bars represent 95% confidence intervals. There was a significant *main effect of PVE bin* for all parameters, indicating an increase in the estimate of each parameter with increasing proportion of GM. There was also a significant *main effect of Group* for CBF, CMRO₂ and D_C, but not for OEF, suggesting consistently lower values of CBF, CMRO₂ and D_C across different GM thresholds in PwMS compared to controls. Finally, there were no significant *interactions PVE bin*Group* for any of the parameters, indicating that GM thresholds have little influence on detecting physiological differences between PwMS and controls. For indication of *p* values, please, see the Results. CBF: cerebral blood flow; OEF: oxygen extraction fraction; CMRO₂: cerebral metabolic rate of oxygen consumption; D_C: capillary oxygen diffusivity.

GM of PwMS compared to matched healthy controls, with no between-group difference for global CBV_{dHb} and OEF. Regional analysis confirmed statistically significant reductions in GM CMRO₂ and D_C in a wide set of cortical regions. Overall, these findings suggest vascular and metabolic dysregulation in PwMS. PmO₂ increase is strongly suggesting mitochondrial energy dysfunction in PwMS. The absence of significant differences in GM

volume between controls and PwMS, suggests that the described changes in tissue physiology may precede significant GM tissue loss in PwMS.

Changes in brain physiology in MS

The observed reductions in GM CBF and CMRO₂ may reflect (i) primary reduction of blood supply at

Table 3. Results of partial volume analysis. Table shows main effect and interaction effects between Group (PwMS, controls) and GM PVE bin.

(p-value)	Main effects				Interaction	
	Group (beta)	Group (beta)	GM PVE bin (p-value)	GM PVE bin (beta)	Group * GM PVE bin (p-value)	Group * GM PVE bin
CBF	-3.24	0.019	4.76	<0.001	-0.34	0.263
OEF	-0.02	0.118	0.01	<0.001	0	0.788
CMRO ₂	-11.18	0.004	13.92	0.001	-1.47	0.089
D _c	-0.27	0.013	0.35	<0.001	-0.04	0.101

CBF: cerebral blood flow, OEF: oxygen extraction fraction, CMRO₂: cerebral metabolic rate of oxygen consumption; D_c: capillary oxygen diffusivity.

the macrovascular level, (ii) microvascular inefficiency in transferring oxygen from the capillary to the mitochondria, (iii) reduced demand for nutrients including oxygen, or (iv) an inability of the tissue to use metabolic substrates for energy release.

The first explanation is unlikely, given that D_c is reduced, suggesting that the reduction in CMRO₂ is associated with local impairment of oxygen diffusion or use at the capillary bed rather than with global change in blood supply.^{2,48,49} The primary modulators of the effective oxygen diffusivity at the capillary bed (D_c) are capillary density and the mitochondrial oxygen tension (PmO₂). Our results report normal microvascular CBV and an increase in PmO₂. Thus, our findings suggest that D_c is reduced in this cohort either due to reduced demand for oxygen, or a reduced capacity for oxygen metabolism.

Histotoxic hypoxia has been identified in MS and referred to as virtual hypoxia.¹⁶ Altered energy production underlying virtual hypoxia may be due to soluble mediators of inflammation that impair mitochondrial function⁵⁰ or to oxidative damage to mitochondrial DNA that may further disrupt mitochondrial activity,⁵¹ ultimately leading to tissue degeneration.¹⁷ Diffuse hypoxia may be a critical pathological mechanism in MS, as the hypoxic and inflammatory responses are intimately linked:⁵² hypoxia exacerbates the inflammatory response⁵³ and inflammation can damage the vascular endothelium, reduce vasoreactivity and promote the influx of leucocytes. In acute inflammation, an increased metabolic demand from inflammatory cells may also increase oxidative stress and exacerbate hypoxia. This cascade of events may chronically lead to further tissue damage and disability.

Our findings of increased PmO₂ in PwMS are consistent with prior research, where alterations in mitochondrial function may result from focal lesion-based hypoxic-like injury, or 'virtual hypoxia'.^{16,54,55} There are two key perspectives on this. First, inflammation associated with NO production and/or defective oxidative phosphorylation can result in reduced ATP

production, leading to an energy-deficient metabolic crisis and subsequent neurodegeneration.^{16,50} Second, mitochondrial energy deficiency coupled with an increase in local energy demand (due to leaky Na⁺ channels) results in chronic starving of mitochondria and leads to axonal degeneration. Our findings in the human brain show increased PmO₂ in the presence of reduced CMRO₂ and CBF, thus possibly reflecting the inability for metabolic substrates to be utilised in the MS brain. However, our findings of intact cognitive ability in PwMS, supports the idea that reductions in energy demand and subsequent neurodegeneration occur prior to the onset of significant cognitive alterations. This mechanism may be a key target for therapies that aim to prevent further neurodegeneration and downstream cognitive decline.

Regional analysis confirmed CMRO₂ and D_c reductions to be widespread across the cortex, with the most significant reductions localised around the cingulate and frontal cortices.⁵⁶ Typically, MS lesions are localised particularly in periventricular WM, which would significantly affect the tracts connecting key frontal and cingulate regions. The localisation of WM damage may make these cortical regions more susceptible to degeneration.^{17,57} We did not observe any significant regional differences in CBV_{dHb}, CBF or OEF. Earlier studies suggest that alterations in OEF may contribute to lower CMRO₂ in PwMS.^{2,58} While we did observe significant reductions in CMRO₂ (globally and regionally) in PwMS, we observed only a slightly lower OEF, the reduction not being statistically significant. One likely explanation for this may be that OEF differences increase with disease duration. Typically, larger OEF reductions have been observed in patients with a longer disease duration (e.g.⁵⁸) whereas smaller OEF reductions have been reported in patients with shorter disease durations (e.g.² and our study). We suggest that further research is needed to establish the trajectory of changes in OEF across disease duration and its potential impact on metabolic dysfunction.

We considered the possibility that partial volume differences between the groups might bias our results and compared physiological estimates as a function of GM partial volumes. We only included a GM partial volume up to 0.8, as there is a limited number of voxels exhibiting higher GM partial volume estimates in some anatomical regions. As expected, estimated regional values of physiological parameters increased as the proportion of GM increased. The CBF, CMRO₂, and D_C differences between PwMS and controls were robust to GM PV variation, suggesting that the observed group differences reflect aspects of tissue physiology that are over and above any potential tissue loss. This is an important result because it suggests that the alterations in the observed physiological state of tissue in MS are not an artefact of altered voxel sampling between the groups but instead the extant GM tissue function is altered in MS.

Relationship between brain physiology, damage and disability

Our results demonstrated that a greater T2 lesion volume is associated with lower CBF and CMRO₂ in GM, consistently with previous findings.² It has been suggested that higher WM lesion burden reflects higher GM lesion load.^{59–61} However, such a relationship is not clearly established⁶² and future studies looking at GM physiology in MS could benefit from the inclusion of scans more sensitive to GM damage and myelination.⁶³

Our data indicated no association between disability scales and tissue physiological status. Lack of direct correlations between behavioural and physiological measures may arise from the presence of adaptation to underlying tissue dysfunction and damage that modulates behavioural performance.⁶⁴ While adaptation may confound the relationship between disability measures and brain physiology, we speculate that tissue physiology may be predictive of future tissue damage and behavioural alterations, an avenue that remains to be explored.

Potential limitations of the study

Our results should be considered in the light of the following limitations. Given that our calibrated fMRI method relies on arterial spin labelling based measurements of CBF, we are only able to reliably estimate physiological parameters in the GM. This limits the comparisons we can make with other studies that summarise global oxygen metabolic changes combined across GM and WM.^{2,18,48} Regional differences in the significance of CMRO₂ and D_C reductions may arise not only from disease effects, but also from variation in

the sensitivity of the technique that is dependent on regional within- and between-subject variation of BOLD and CBF measurements. The scans that we used to identify lesions are not generally sensitive to lesions within GM. Therefore, our reported associations between lesion load and GM physiology are limited to WM lesions only. In addition, PmO₂ results were found assuming parameters related to tissue and vascular topology are fixed. Tissue and vascular remodelling in PwMS might have introduced some bias into the results. Further studies should be performed to address this topic.

Conclusions

Our findings suggest that an oxygen metabolic dysregulation occurs in MS patients, resulting in reduced cerebral blood flow and oxygen utilisation. These changes may precede GM tissue loss, thereby suggesting potentially promising mechanisms to be targeted in the development of neuroprotective interventions. The use of a multi-parametric dc-fMRI approach can provide valuable quantitative data regarding altered brain physiology in MS and, with a regional approach, may help identify areas of early tissue dysfunction and monitoring their subsequent evolution.

Funding

The author(s) disclosed receipt of the following financial support for the research, authorship, and/or publication of this article: This project was supported by the UK Engineering and Physical Sciences Research Council (grant numbers EP/K020404/1 and EP/S025901/1). HLC, SK and MG were funded by a Wellcome Strategic Award to CUBRIC, 'Multi-scale and multi-modal assessment of coupling in the healthy and diseased brain', grant reference 104943/Z/14/Z. MG thanks the Wellcome Trust for its support via a Sir Henry Dale Fellowship (220575/Z/20/Z). RS, CF and EP were supported by a Wellcome PhD studentships.

Acknowledgements

For the purpose of Open Access, the author has applied a CC BY public copyright licence to any Author Accepted Manuscript version arising from this submission. We thank the patients with MS and their families, along with the healthy volunteers, for their time and support that made this research possible.

Authors' contributions

Writing manuscript – HLC, RGW, MG, VT
Data collection – HLC, RS, EP
Study design – HLC, RS, CF, RGW, VT
Data analysis – HLC, TML, RS, AMC, EP.
Clinical support – NS, SK
Lead clinician – VT
PI – RGW, VT.

Data availability statement

We do not have ethical consent to make the in-vivo participant datasets acquired for this study publicly available in an unrestricted manner. However, the authors may be contacted for collaborative research enquiries involving the data presented.


Declaration of conflicting interests

The author(s) declared the following potential conflicts of interest with respect to the research, authorship, and/or publication of this article: VT has received honoraria for consultancy, travel and research grants from Biogen, Merck Serono, Viatris, Allmiral, Bristol Myers Squibb, Novartis, Sanofi. The other authors declare no competing interests.

ORCID iDs

Rachael C Stickland  <https://orcid.org/0000-0003-3398-4272>

Michael Germuska  <https://orcid.org/0000-0003-0580-4350>

Antonio M Chiarelli  <https://orcid.org/0000-0002-5347-8417>

References

1. Paling D, Golay X, Wheeler-Kingshott C, et al. Energy failure in multiple sclerosis and its investigation using MR techniques. *J Neurol* 2011; 258: 2113–2127.
2. Ge Y, Zhang Z, Lu H, et al. Characterizing brain oxygen metabolism in patients with multiple sclerosis with T2-relaxation-under-spin-tagging MRI. *J Cereb Blood Flow Metab* 2012; 32: 403–412.
3. Wuerfel J, Bellmann-Strobl J, Brunecker P, et al. Changes in cerebral perfusion precede plaque formation in multiple sclerosis: a longitudinal perfusion MRI study. *Brain* 2004; 127: 111–119.
4. Debernard L, Melzer TR, Van Stockum S, et al. Reduced grey matter perfusion without volume loss in early relapsing-remitting multiple sclerosis. *J Neurol Neurosurg Psychiatry* 2014; 85: 544–551.
5. Marshall O, Chawla S, Lu H, et al. Cerebral blood flow modulation insufficiency in brain networks in multiple sclerosis: a hypercapnia MRI study. *J Cereb Blood Flow Metab* 2016; 36: 2087–2095.
6. Marshall O, Lu H, Brisset JC, et al. Impaired cerebrovascular reactivity in multiple sclerosis. *Jama Neurol* 2014; 71: 1275–1281.
7. Pelizzari L, Lagana MM, Baglio F, et al. Cerebrovascular reactivity and its correlation with age in patients with multiple sclerosis. *Brain Imaging Behav* 2020; 14: 1889–1898.
8. Brooks DJ, Leenders KL, Head G, et al. Studies on regional cerebral oxygen utilisation and cognitive function in multiple sclerosis. *J Neurol Neurosurg Psychiatry* 1984; 47: 1182–1191.
9. Sun X, Tanaka M, Kondo S, et al. Reduced cerebellar blood flow and oxygen metabolism in spinocerebellar degeneration: a combined PET and MRI study. *J Neurol* 1994; 241: 295–300.
10. Sun X, Tanaka M, Kondo S, et al. Clinical significance of reduced cerebral metabolism in multiple sclerosis: a combined PET and MRI study. *Ann Nucl Med* 1998; 12: 89–94.
11. Paulesu E, Perani D, Fazio F, et al. Functional basis of memory impairment in multiple sclerosis: a[18F]FDG PET study. *Neuroimage* 1996; 4: 87–96.
12. Pytel V, Matias-Guiu JA, Matias-Guiu J, et al. Amyloid PET findings in multiple sclerosis are associated with cognitive decline at 18 months. *Mult Scler Relat Disord* 2020; 39: 101926.
13. Davies AL, Desai RA, Bloomfield PS, et al. Neurological deficits caused by tissue hypoxia in neuroinflammatory disease. *Ann Neurol* 2013; 74: 815–825.
14. Law M, Saindane AM, Ge Y, et al. Microvascular abnormality in relapsing-remitting multiple sclerosis: perfusion MR imaging findings in normal-appearing white matter. *Radiology* 2004; 231: 645–652.
15. Yang R and Dunn JF. Reduced cortical microvascular oxygenation in multiple sclerosis: a blinded, case-controlled study using a novel quantitative near-infrared spectroscopy method. *Sci Rep* 2015; 5: 16477.
16. Trapp BD and Stys PK. Virtual hypoxia and chronic necrosis of demyelinated axons in multiple sclerosis. *Lancet Neurol* 2009; 8: 280–291.
17. Haider L, Zrzavy T, Hametner S, et al. The topography of demyelination and neurodegeneration in the multiple sclerosis brain. *Brain* 2016; 139: 807–815.
18. West K, Sivakolundu D, Maruthy G, et al. Baseline cerebral metabolism predicts fatigue and cognition in multiple sclerosis patients. *Neuroimage Clin* 2020; 27: 102281.
19. Germuska M and Wise RG. Calibrated fMRI for mapping absolute CMRO₂: practicalities and prospects. *Neuroimage* 2019; 187: 145–153.
20. Gauthier CJ and Hoge RD. A generalized procedure for calibrated MRI incorporating hyperoxia and hypercapnia. *Hum Brain Mapp* 2013; 34: 1053–1069.
21. Wise RG, Harris AD, Stone AJ, et al. Measurement of OEF and absolute CMRO₂: MRI-based methods using interleaved and combined hypercapnia and hyperoxia. *Neuroimage* 2013; 83: 135–147.
22. Bulte DP, Kelly M, Germuska M, et al. Quantitative measurement of cerebral physiology using respiratory-calibrated MRI. *Neuroimage* 2012; 60: 582–591.
23. Merola A, Germuska MA, Murphy K, et al. Assessing the repeatability of absolute CMRO₂, OEF and haemodynamic measurements from calibrated fMRI. *Neuroimage* 2018; 173: 113–126.
24. Germuska M, Chandler H, Okell T, et al. A frequency-domain machine learning method for dual-calibrated fMRI mapping of oxygen extraction fraction (OEF) and cerebral metabolic rate of oxygen consumption (CMRO₂). *Front Artif Intell* 2020; 3
25. Germuska M, Chandler HL, Stickland RC, et al. Dual-calibrated fMRI measurement of absolute cerebral

- metabolic rate of oxygen consumption and effective oxygen diffusivity. *Neuroimage* 2019; 184: 717–728.
26. Germuska M, Merola A, Murphy K, et al. A forward modelling approach for the estimation of oxygen extraction fraction by calibrated fMRI. *Neuroimage* 2016; 139: 313–323.
 27. Hoge RD. Calibrated FMRI. *Neuroimage* 2012; 62: 930–937.
 28. Merola A, Germuska MA, Warnert EA, et al. Mapping the pharmacological modulation of brain oxygen metabolism: the effects of caffeine on absolute CMRO₂ measured using dual calibrated fMRI. *Neuroimage* 2017; 155: 331–343.
 29. Thompson AJ, Banwell BL, Barkhof F, et al. Diagnosis of multiple sclerosis: 2017 revisions of the McDonald criteria. *Lancet Neurol* 2018; 17: 162–173.
 30. Lublin FD, Reingold SC, Cohen JA, et al. Defining the clinical course of multiple sclerosis: the 2013 revisions. *Neurology* 2014; 83: 278–286.
 31. Cutter GR, Baier ML, Rudick RA, et al. Development of a multiple sclerosis functional composite as a clinical trial outcome measure. *Brain* 1999; 122: 871–882.
 32. Benedict RHB, DeLuca J, Phillips G, Multiple Sclerosis Outcome Assessments Consortium, et al. Validity of the symbol digit modalities test as a cognition performance outcome measure for multiple sclerosis. *Mult Scler* 2017; 23: 721–733.
 33. Hobart J, Lamping D, Fitzpatrick R, et al. The multiple sclerosis impact scale (MSIS-29): a new patient-based outcome measure. *Brain* 2001; 124: 962–973.
 34. Penner IK, Raselli C, Stocklin M, et al. The fatigue scale for motor and cognitive functions (FSMC): validation of a new instrument to assess multiple sclerosis-related fatigue. *Mult Scler* 2009; 15: 1509–1517.
 35. Kurtzke JF. Rating neurologic impairment in multiple sclerosis: an expanded disability status scale (EDSS). *Neurology* 1983; 33: 1444–1452.
 36. Schmithorst VJ, Hernandez-Garcia L, Vannest J, et al. Optimized simultaneous ASL and BOLD functional imaging of the whole brain. *J Magn Reson Imaging* 2014; 39: 1104–1117.
 37. Okell TW, Chappell MA, Kelly ME, et al. Cerebral blood flow quantification using vessel-encoded arterial spin labeling. *J Cereb Blood Flow Metab* 2013; 33: 1716–1724.
 38. Jenkinson M, Beckmann CF, Behrens TE, et al. Fsl. *Neuroimage* 2012; 62: 782–790.
 39. Zhang YY, Brady M and Smith S. Segmentation of brain MR images through a hidden markov random field model and the expectation-maximization algorithm. *Ieee Trans Med Imaging* 2001; 20: 45–57.
 40. Patenaude B, Smith SM, Kennedy DN, et al. A Bayesian model of shape and appearance for subcortical brain segmentation. *Neuroimage* 2011; 56: 907–922.
 41. Smith S, Bannister PR, Beckmann C, et al. FSL: new tools for functional and structural brain image analysis. *Neuroimage* 2001; 13: 249. S.
 42. Smith SM. Fast robust automated brain extraction. *Hum Brain Mapp* 2002; 17: 143–155.
 43. Battaglini M, Jenkinson M and De Stefano N. Evaluating and reducing the impact of white matter lesions on brain volume measurements. *Hum Brain Mapp* 2012; 33: 2062–2071.
 44. Gelineau-Morel R, Tomassini V, Jenkinson M, et al. The effect of hypointense white matter lesions on automated gray matter segmentation in multiple sclerosis. *Hum Brain Mapp* 2012; 33: 2802–2814.
 45. Sargolzaei S, Sargolzaei A, Cabrerizo M, et al. A practical guideline for intracranial volume estimation in patients with alzheimer's disease. *Bmc Bioinformatics* 2015; 16 Suppl 7: S8.
 46. Germuska M, Stickland R, Chiarelli A. et al. Quantitative mapping of cerebral oxygen metabolism using breath-hold calibrated fMRI. *bioRxiv*. 2021: 2021.04.08.438939.
 47. Tzourio-Mazoyer N, Landeau B, Papathanassiou D, et al. Automated anatomical labeling of activations in SPM using a macroscopic anatomical parcellation of the MNI MRI single-subject brain. *Neuroimage* 2002; 15: 273–289.
 48. Fan AP, Govindarajan ST, Kinkel RP, et al. Quantitative oxygen extraction fraction from 7-Tesla MRI phase: reproducibility and application in multiple sclerosis. *J Cereb Blood Flow Metab* 2015; 35: 131–139.
 49. Watchmaker JM, Juttukonda MR, Davis LT, et al. Hemodynamic mechanisms underlying elevated oxygen extraction fraction (OEF) in moyamoya and sickle cell anemia patients. *J Cereb Blood Flow Metab* 2018; 38: 1618–1630.
 50. Mahad DH, Trapp BD and Lassmann H. Pathological mechanisms in progressive multiple sclerosis. *Lancet Neurol* 2015; 14: 183–193.
 51. Lu F, Selak M, O'Connor J, et al. Oxidative damage to mitochondrial DNA and activity of mitochondrial enzymes in chronic active lesions of multiple sclerosis. *J Neurol Sci* 2000; 177: 95–103.
 52. Yang R and Dunn JF. Multiple sclerosis disease progression: contributions from a hypoxia-inflammation cycle. *Mult Scler* 2019; 25: 1715–1718.
 53. Snyder B, Shell B, Cunningham JT, et al. Chronic intermittent hypoxia induces oxidative stress and inflammation in brain regions associated with early-stage neurodegeneration. *Physiol Rep* 2017; 5: e13258.
 54. Redford EJ, Kapoor R and Smith KJ. Nitric oxide donors reversibly block axonal conduction: demyelinated axons are especially susceptible. *Brain* 1997; 120: 2149–2157. (Pt
 55. Aboul-Enein F and Lassmann H. Mitochondrial damage and histotoxic hypoxia: a pathway of tissue injury in inflammatory brain disease? *Acta Neuropathol* 2005; 109: 49–55.
 56. Eshaghi A, Marinescu RV, Young AL, et al. Progression of regional grey matter atrophy in multiple sclerosis. *Brain* 2018; 141: 1665–1677.

57. Charil A, Dagher A, Lerch JP, et al. Focal cortical atrophy in multiple sclerosis: relation to lesion load and disability. *Neuroimage* 2007; 34: 509–517.
58. Cho J, Nguyen TD, Huang W, et al. Brain oxygen extraction fraction mapping in patients with multiple sclerosis. *J Cereb Blood Flow Metab* 2022; 42: 338–348.
59. Muhlau M, Buck D, Forschler A, et al. White-matter lesions drive deep gray-matter atrophy in early multiple sclerosis: support from structural MRI. *Mult Scler* 2013; 19: 1485–1492.
60. Steenwijk MD, Geurts JJ, Daams M, et al. Cortical atrophy patterns in multiple sclerosis are non-random and clinically relevant. *Brain* 2016; 139: 115–126.
61. Bodini B, Khaleeli Z, Cercignani M, et al. Exploring the relationship between white matter and gray matter damage in early primary progressive multiple sclerosis: an in vivo study with TBSS and VBM. *Hum Brain Mapp* 2009; 30: 2852–2861.
62. Calabrese M, Romualdi C, Poretto V, et al. The changing clinical course of multiple sclerosis: a matter of gray matter. *Ann Neurol* 2013; 74: 76–83.
63. Abidi Z, Faeghi F, Mardanshahi Z, et al. Assessment of the diagnostic accuracy of double inversion recovery sequence compared with FLAIR and T2W_TSE in detection of cerebral multiple sclerosis lesions. *Electron Physician* 2017; 9: 4162–4170.
64. Tomassini V, Matthews PM, Thompson AJ, et al. Neuroplasticity and functional recovery in multiple sclerosis. *Nat Rev Neurol* 2012; 8: 635–646.